Appl. Phys. B 92, 73–77 (2008)
DOI: 10.1007/s00340-008-3068-5

Applied Physics B
Lasers and Optics

A. TAKAHASHI[1,✉]
D. NAKAMURA[2]
K. TAMARU[2]
T. AKIYAMA[2]
T. OKADA[2]

Emission characteristics of debris from CO_2 and Nd:YAG laser-produced tin plasmas for extreme ultraviolet lithography light source

[1] Department of Health Sciences, School of Medicine, Kyushu University, 3-1-1, Maidashi, Higashi-ku, Fukuoka 812-8582, Japan
[2] Department of Electrical and Electronic System Engineering, Graduate School of Information Science and Electrical and Electronic System Engineering, Kyushu University, 774, Motooka, Nishi-ku, Fukuoka 819-0395, Japan

Received: 11 December 2007 / Revised version: 2 May 2008
Published online: 13 June 2008 •

ABSTRACT We describe a comparative study of the emission characteristics of debris from CO_2 and Nd:YAG laser-produced tin plasmas for developing an extreme-ultraviolet (EUV) lithography light source. Tin (Sn) ions and droplets emitted from a Sn plasma produced by a CO_2 laser or an Nd:YAG laser were detected using Faraday cups and quartz crystal microbalance (QCM) detectors, respectively. The droplets were also monitored by using silicon substrates as witness plates. The results showed higher ion kinetic energy and lower particle emission for the CO_2 laser than the Nd:YAG laser for the same laser energy (50 mJ). The average ion energy was 2.2 keV for the CO_2 laser-produced plasma (LPP), and 0.6 keV for the Nd:YAG LPP. The debris accumulation of the CO_2 LPP detected by the QCM detectors, however, was less than one fourth of that of the Nd:YAG LPP for the same laser energy. Using ion energy data, the mirror lifetime is estimated for the CO_2 and Nd:YAG lasers. In both cases, the upper limit of the number of shots was of the order of 10^6.

PACS 52.38.DX; 52.38.Ph; 52.38.Mf

1 Introduction

An extreme-ultraviolet (EUV) light source has been developed as a next-generation lithography tool for the manufacture of micro-devices with nano-scale electronic nodes. A practical EUV lithography light source requires EUV power as high as 115–180 W in a 2% bandwidth around 13.5 nm [1, 2]. The 13.5 nm light is produced by the hot plasmas of a target material. Laser-produced plasma (LPP) and discharge-produced plasma (DPP) are the two approaches currently under development [1]. These competing approaches have some common issues: the conversion efficiency of deposited energy into the 13.5 nm light, out-of-band radiation [19], and debris (high-energy ions, atoms, and micro-droplets) emitted from the plasma. The debris damages the expensive and delicate multilayer mirror which is composed of molybdenum (Mo) and silicon (Si), and reduces its reflectivity. Low-energy particles accumulate on the mirror surface, whereas high-energy particles erode the mirror surface.

✉ Fax: +81-92-642-6674, E-mail: takahashi@shs.kyushu-u.ac.jp

The choice of target material is important because both conversion efficiency and debris emission depend on the material. The most promising target material at present is tin (Sn). A conversion efficiency of $\sim 3\%$ has been obtained for Sn; this is higher than that for any other material, such as xenon (Xe) or lithium (Li). However, the problem of debris emission is more critical in the case of Sn; therefore, various measures against debris have been proposed and attempted [2, 8, 9]. The emission characteristics of debris should be fully understood to develop an efficient shield. The characteristics of debris emission in a DPP were reported by Srivastava et al. [3]. They measured the energy and ion flux emitted from a z-pinch source, fueled by Xe and $SnCl_4$, and estimated the lifetime of the collector optics using the obtained results [3]. For LPP, some researchers have reported the debris emission characteristics and showed interesting results [9, 11–14]; currently, almost all of the investigations are based on the Nd:YAG LPP.

The early research on LPP for the 13.5 nm EUV light source focused only on Nd:YAG LPP. The CO_2 laser, which is an alternative high-power laser, was not considered since many researchers thought that the energy deposited into the produced plasma was too small to produce hot and dense plasmas, because of the low cut-off plasma density ($\sim 10^{19}$ cm^{-3}), due to the long wavelength (10.6 μm). In general, there is an optimum plasma temperature and density for effective 13.5 nm emission. For example, the optimum temperature of a Xe plasma is approximately 30 eV, which is easily achievable with a CO_2 laser. Excessively hot plasma decreases the conversion efficiency, because the ions are excited to higher energy levels and the side bands around the 13.5 nm line increase. In addition, excessively dense plasma also decreases the conversion efficiency due to self-absorption of the 13.5 nm emission in the plasma; therefore, a short-wavelength laser is not suitable for efficient EUV generation.

Based on these considerations, we proposed a CO_2 LPP, and showed that the conversion efficiency of a CO_2 laser-produced tin plasma is comparable to that of the Nd:YAG laser [4–6]. CO_2 LPP has become more important in the development of EUV lithography light sources since our first demonstration [9, 10], and it is important to investigate its characteristics including debris emission. In our previous study, we investigated the behavior of neutral Sn atoms using laser-induced fluorescence (LIF) imaging [7, 8], where we vi-

sualized the spatial distributions of Sn atoms and the sputtering of a dummy mirror by fast ions generated from a Nd:YAG laser-produced tin plasma. In this study, we investigate the emission characteristics of Sn ions and micro-droplets from CO_2 and Nd:YAG laser-produced tin plasmas for a 13.5 nm EUV light source, and compare their characteristics. Using this data, we calculate mirror damage.

2 Experimental setup

Figure 1 shows the experimental arrangement. All devices, except the plasma shutter (PS), were placed inside a chamber, and the chamber was pumped to a pressure of about 3×10^{-3} Pa. The CO_2 and Nd:YAG laser beams were focused on a rotating Sn plate by a lens with a focal length of 150 mm. The Nd:YAG laser (SPECTRA PHYSICS Quanta-Ray PRO) is Q-switched, and its pulse width is 8 ns full width half maximum (FWHM). The CO_2 laser (LAMBDA PHYSIK EMG201MSC) has an unstable resonator and a spike pulse, with a pulse width of 50 ns FWHM and a long tail, as represented by the dashed line in Fig. 2.

The energy spectrum of ions from the Sn plasma is measured using four Faraday cups (FCs) placed around the Sn target; the cups capture the angle distribution for a single shot. The distance between the FC and the Sn target is 110 mm, which is comparable to a real environment for high volume manufacturing production. The amount of debris and droplets are measured using four quartz crystal microbalance (QCM) detectors and Si substrates (10×10 mm^2) as shown by plates mounted at the same positions as the FCs. The QCM surface material was gold.

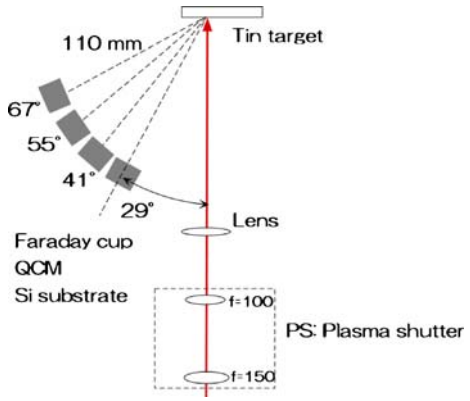

FIGURE 1 Schematic of the experimental arrangement

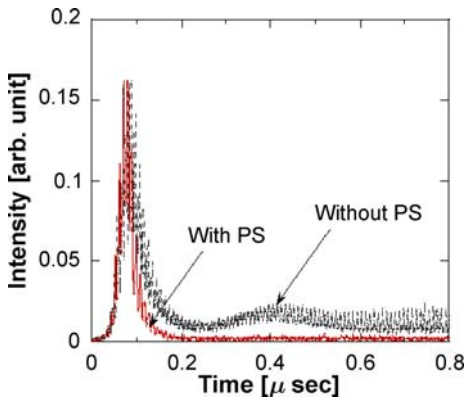

FIGURE 2 Pulse shape of the CO_2 laser without PS (*dashed line*) and with PS (*solid line*)

3 Experimental results

3.1 *Characteristics of ion kinetic energy*

Figure 3 shows the ion signals detected by the FCs from the Nd:YAG and CO_2 laser-produced tin plasmas. The peak laser intensity was 2×10^{10} W/cm^2 for the Nd:YAG laser and 1×10^{10} W/cm^2 for the CO_2 laser. The energies were 50 and 160 mJ, respectively. These intensities are not optimal for obtaining maximum conversion efficiency; however, the efficiencies in both cases are similar, judging from our previous study [6]. Although the intensity of the Nd:YAG laser is about twice that of the CO_2 laser, these signals suggest that the ion kinetic energy of the CO_2 LPP is higher than that of the Nd:YAG LPP. The ion signal of the CO_2 LPP has a complex structure; and the time axis would not correspond to the time-of-flight of the ions, if the ions were generated by the latter half of the laser pulse.

To avoid complex analysis and to investigate the effect of the laser pulse shape, we arranged a plasma shutter (PS) outside the chamber to cut off the tail of the CO_2 laser pulse, as shown in Fig. 1. The PS is composed of a pair of lenses. The laser beam produces a plasma at the focal point, and the plasma absorbs the latter half of the beam. The compressed pulse shape is described by the solid line shown in Fig. 2. The tail is cut off, and the pulse width is shortened to 20 ns FWHM.

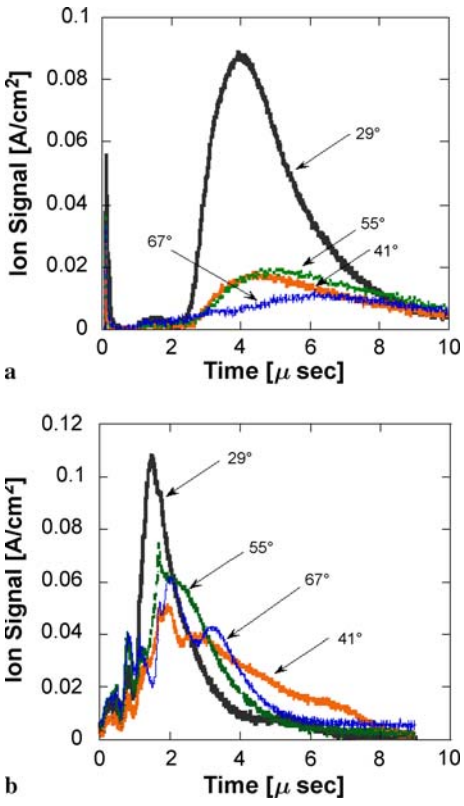

FIGURE 3 Ion signals from (**a**) Nd:YAG and (**b**) CO_2 laser-produced tin plasmas without PS

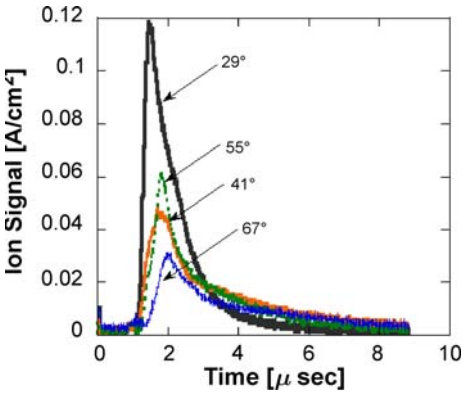

FIGURE 4 Ion signals from CO_2 laser-produced tin plasma with PS

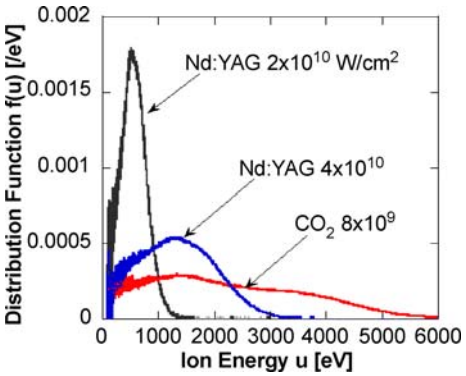

FIGURE 5 Ion energy spectra of Nd:YAG and CO_2 laser-produced tin plasmas

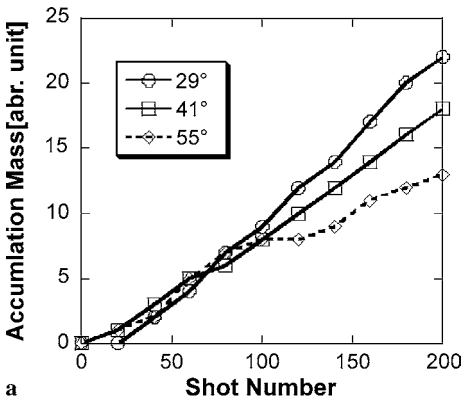

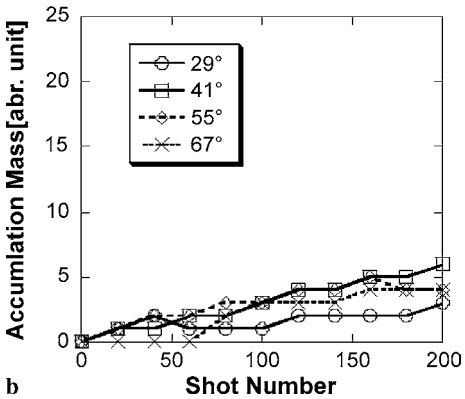

FIGURE 6 Debris accumulation from (**a**) Nd:YAG and (**b**) CO_2 laser-produced tin plasmas

The ion signal with the compressed pulse is shown in Fig. 4. The peak intensity was about 8×10^9 W/cm^2 and the energy was 50 mJ. The effect is obvious: the initial signal around 1 μs and the later signal, after 3 μs, disappeared. This result suggests that the tail of the CO_2 laser pulse generates both low- and high-energy ions. Figure 5 shows the ion kinetic energy distributions $f(u)$ in eV^{-1} at 29° from the target normal; these are derived from the signals in Figs. 3a and 4. It is obvious that the ion kinetic energy of the CO_2 LPP is higher than that of the Nd:YAG LPP. The average ion energy, obtained from

$$\overline{u} = \int_0^\infty u\, f(u)\, \mathrm{d}u\,, \tag{1}$$

is 0.6 keV for the Nd:YAG LPP, and 2.2 keV for the CO_2 LPP. For reference, Fig. 5 also shows the ion energy distribution of the Nd:YAG LPP when the laser intensity was 4×10^{10} W/cm^2. The average energy is 1.2 keV.

3.2 *Characteristics of debris accumulation*

In the experiments mentioned in this section, the laser intensity was the same as in Figs. 3a and 4. Figure 6 shows the debris accumulation measured by QCM for each shot number. The debris accumulation increased with the number of shots. Note that the debris emission of the CO_2 LPP was less than one-fourth that of the Nd:YAG LPP for the same laser energy. The accumulation was smallest at 29°, with the CO_2 LPP. We believe that the Sn deposited onto the QCM detectors at 29° was spattered by high-energy Sn ions. In our previous study, we visualized the images of Sn atoms spattered from a tin-deposited silicon plate, using laser-induced florescence [7, 8].

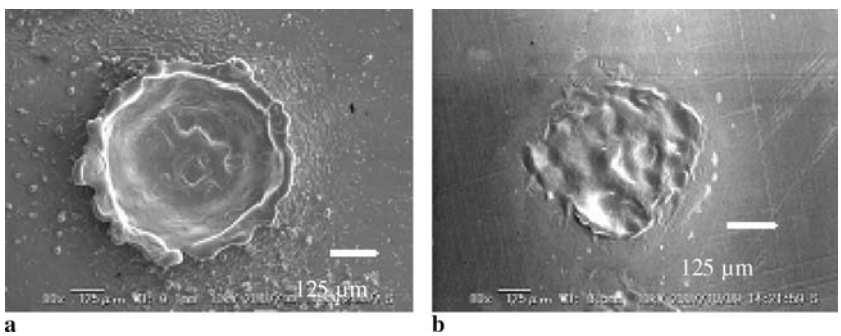

FIGURE 7 Electron microscope image of surface of a Sn target. (**a**) Nd:YAG laser and (**b**) CO_2 laser

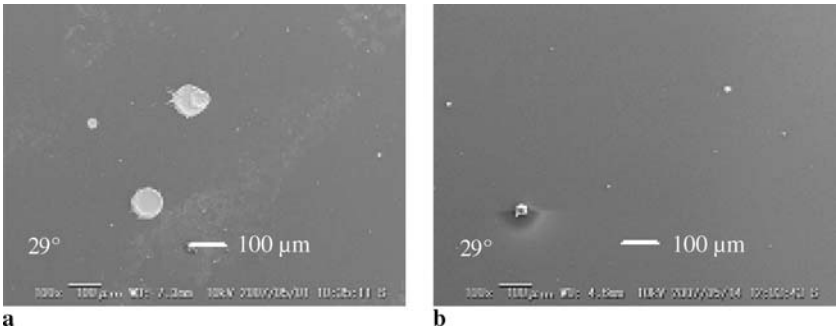

a b

FIGURE 8 Electron microscope image of the surface of a Si plate mounted at an angle of 29° from the target normal. (**a**) Nd:YAG laser and (**b**) CO_2 laser

Figure 7 shows the electron microscope images of a tin target surface irradiated twenty times by a short-pulse CO_2 and an Nd:YAG lasers. The deep crater is trenched in the case of the Nd:YAG LPP, and this image shows that a large amount of tin was spattered. In addition, Fig. 8 shows an electron microscope image of the surface of the silicon substrate. The droplet sizes for the Nd:YAG LPP was much larger than those for the CO_2 LPP. The images shown in Figs. 7 and 8 support the result shown in Fig. 6.

4 Discussion

Here, the experimental results are discussed and interpreted in terms of the interaction between the laser pulse and the produced plasma. The dominant absorption process in long-wavelength lasers is Joule heating, where electrons accelerated by the laser field collide inelastically with ions or neutral atoms. The Joule heating absorption coefficient is proportional to ω^{-2}, where ω is the angular frequency of the laser [15, 16], expressed as follows:

$$Q_J = \frac{e^2}{m}\frac{\nu E^2}{\nu^2+\omega^2} \approx \frac{e^2}{m}\frac{\nu E^2}{\omega^2}\,, \tag{2}$$

where e is electron charge, m is electron mass, E is laser electric field, and ν is collision frequency. Equation (2) indicated that the absorption efficiency of the CO_2 laser field is higher than that of the Nd:YAG laser by two orders of magnitude. The CO_2 laser is absorbed in the superficial low-density region of the plasma; therefore, the energy deposited per electron is larger, and the electron temperature at the plasma surface should be higher than that in the case of the Nd:YAG LPP. The superficial high-energy electrons would rapidly scatter, and produce an electric field to accelerate the ions. The electric field becomes larger with increasing initial electron temperature [17, 18]. The initial high electron temperature is responsible for the high ion energy in the case of the CO_2 LPP.

Another reason is the energy loss due to collisions between ions and other particles. The accelerated ions will collide with the particles around them, and thus lose kinetic energy. In the case of the CO_2 LPP, since the ions are generated in the superficial low-density region, the collision energy loss of ions will be less than that in the case of the Nd:YAG LPP. This also explains the high-energy ion signals shown in Fig. 3b. We believe that the tail of the CO_2 laser pulse was efficiently absorbed in the expanded low-density plume and generated high-energy ions. When the plasma shutter cut the tail, the high-energy signal disappeared.

The characteristic of debris emission, shown in Figs. 6 and 7, is also attributed to the absorption mechanism of the laser energy. In the case of the Nd:YAG LPP, the laser penetrates up to the target surface, the target surface is superheated into a liquid phase, and droplets are formed. In contrast, for the CO_2 LPP, once the plasma is produced, the energy is absorbed in the plasma surface; therefore, the target surface is not heated as much as by the Nd:YAG LPP.

Figures 3 and 4 suggest that the Nd:YAG LPP produces more ions with low-energies, on the other hand, the CO_2 LPP produces fewer ions with high-energies. We now consider which of these two phenomena is more harmful to the optics. To estimate the effect on the collector mirror, we calculate the multilayer mirror erosion due to ions. The ion flux required to remove a given thickness of a substance is

$$\Gamma_i = \frac{\Delta_i n_i}{Y_i}\,, \tag{3}$$

where Δ_i is thickness of the substance, n_i is the number density of the substance, Y_i is sputtering yield, and subscript (i) denotes the multilayer substance (Mo, Si). The sputtering yield, which is calculated using SRIM2008, depends on the ion energy. We adopted the average energy calculated by (1) (3 keV for the CO_2 LPP and 1 keV for the Nd:YAG LPP). Table 1 shows the substrate data and the calculation results.

The ion flux emitted from the LPP per pulse is

$$\gamma = \frac{j_\mathrm{p}\tau}{e}\,, \tag{4}$$

where j_p (A/cm^2) is the peak ion current density shown in Figs. 3a and 4, τ (s) is the FWHM of the ion current, and e is electron charge (1.602×10^{-19} C). Using (4), the ion flux of the Nd:YAG LPP (γ_YAG) or CO_2 LPP (γ_{CO_2}) at 29° is calculated to be 1.7×10^{12} ions/cm^2 for the Nd:YAG LPP and

	Δ_i (nm)	n_i (cm^{-3})	Y_i (0.6 keV for Nd:YAG) (atoms/ion)	Y_i (2.2 keV for CO_2) (atoms/ion)	Γ_i (0.6 keV) (ions/cm^2)	Γ_i (2.2 keV) (ions/cm^2)
Mo	2.76	6.41×10^{22}	0.628	1.66	2.82×10^{16}	1.07×10^{16}
Si	4.14	4.98×10^{22}	0.109	0.391	1.89×10^{17}	5.27×10^{16}

TABLE 1 Material data for Mo and Si and calculation results of Y_i and Γ_i

7.5×10^{11} ions/cm^2 for the CO_2 LPP. The number of shots required to remove one bilayer of Mo-Si is $(\Gamma_{Mo} + \Gamma_{Si})/\gamma_{YAG} = (2.82 \times 10^{16} + 1.89 \times 10^{17})/1.7 \times 10^{12} = 1.3 \times 10^5$ shots for the Nd:YAG LPP, and $(\Gamma_{Mo} + \Gamma_{Si})/\gamma_{CO_2} = (1.07 \times 10^{16} + 5.27 \times 10^{16})/7.5 \times 10^{11} = 8.5 \times 10^4$ shots for the CO_2 LPP.

Srivastava et al. assumed that the limit of reflectivity loss is 10% of the optimum value, and showed that the erosion of 25 bilayers decreases the reflectivity down to its limit [3]. Adopting their definition, the upper limit for the number of shots is $N \times 25 = 3.3 \times 10^6$ shots for the Nd:YAG LPP and 2.1×10^6 shots for the CO_2 LPP. It should be noted that the upper limit of the CO_2 LPP is similar to that of the Nd:YAG LPP despite the higher ion energy. This is because the ion flux of the Nd:YAG LPP is larger than that of the CO_2 LPP; in other words, the former produces more ions with low-energy.

However, the mirror lifetime assumed above is much shorter than that in the case of DPP [3]; therefore, it is essential to take measures against erosion. Promising techniques in this regard include a magnetic shield [9] and an H_2 trap [8]. This consideration does not take into account the accumulation processes; however, the results in Fig. 6 apparently show that the damage done to the mirror by the CO_2 LPP should be less than that by the Nd:YAG LPP.

5 Summary

In summary, a comparative study on the emission characteristics of debris from laser-produced tin plasmas was conducted using two different lasers: an Nd:YAG laser and a CO_2 laser. A higher ion kinetic energy and a lower droplet emission were observed for the CO_2 laser compared with the Nd:YAG laser at the same laser energy. The interaction of the laser pulse with the plasma is responsible for these characteristics. The deposited energy density of the CO_2 laser is considerably larger than that of the Nd:YAG laser for the same laser energy, because the CO_2 laser is absorbed in the superficial region of the plasma, due to its long wavelength; in contrast, the Nd:YAG laser deeply penetrates the plasma. This causes a higher ion energy and complete vaporization of the target material in the case of the CO_2 laser. Using the ion energy data, the lifetime of the mirror is calculated for the CO_2 and Nd:YAG LPP. The predicted damage caused to the mirror due to ion erosion in the case of the former is at the same level as that of the latter despite the higher ion energy.

ACKNOWLEDGEMENTS This study was performed under the auspices of the MEXT (Ministry of Education, Culture, Science and Technology, Japan) under a contract subject "Leading Project for EUV lithography source development."

REFERENCES

1 J. Jonkers, Plasma Source Sci. Technol. **15**, S8 (2006)
2 K. Kemp, S. Wurm, C.R. Physique **7**, 875 (2006)
3 S.N. Srivastava, K.C. Thompson, E.L. Antonsen, H. Qiu, J.B. Spencer, D. Papke, D.N. Ruzic, J. Appl. Phys. **102**, 023 301 (2007)
4 H. Tanaka, K. Akinaga, A. Takahashi, T. Okada, Proc. SPIE **5662**, 313 (2004)
5 H. Tanaka, K. Akinaga, A. Takahashi, T. Okada, Proc. SPIE **5662**, 361 (2004)
6 H. Tanaka, A. Matsumoto, K. Akinaga, A. Takahashi, T. Okada, Appl. Phys. Lett. **87**, 04 153 (2005)
7 H. Tanaka, Y. Hashimoto, K. Tamaru, A. Takahashi, T. Okada, Appl. Phys. Lett. **89**, 181 109 (2006)
8 D. Nakamura, K. Tamaru, Y. Hashimoto, T. Okada, H. Tanaka, A. Takahashi, J. Appl. Phys. **102**, 123 310 (2007)
9 H. Komori, Y. Ueno, H. Hoshino, T. Ariga, G. Soumagne, A. Endo, H. Mizoguchi, Appl. Phys. B **83**, 213 (2006)
10 Y. Ueno, T. Ariga, G. Soumagne, T. Higashiguchib, S. Kubodera, I. Pogorelsky, I. Pavlishin, D. Stolyarov, M. Babzien, K. Kusche, V. Yakimenko, Appl. Phys. Lett. **90**, 191 503 (2007)
11 Y. Tao, M.S. Tillack, Appl. Phys. Lett. **89**, 111 502 (2006)
12 Y. Tao, M.S. Tillack, S.S. Harilal, K.L. Sequoia, F. Najmabadi, J. Appl. Phys. **101**, 023 305 (2007)
13 T. Higashiguchi, C. Rajyaguru, N. Dojyo, Y. Taniguchi, K. Sakita, S. Kubodera, Rev. Sci. Instrum. **76**, 126 102 (2005)
14 T. Higashiguchi, N. Dojyo, M. Hamada, W. Sasaki, S. Kubodera, Appl. Phys. Lett. **88**, 201 503 (2006)
15 C.H. Chan, C.D. Moody, J. Appl. Phys. **45**, 1105 (1974)
16 A. Takahashi, K. Nishijima, Japan. J. Appl. Phys. **34**, 2471 (1995)
17 M. Murakami, Y.-G. Kang, K. Nishihara, S. Fujioka, H. Nishimura, Phys. Plasmas **12**, 062 706 (2005)
18 M. Murakami, M.M. Basko, Phys. Plasmas **13**, 012 105 (2006)
19 H. Sakaguchi, S. Fujioka, S. Namba, H. Tanuma, H. Ohashi, S. Suda, M. Shimomura, Y. Nakai, Y. Kimura, Y. Yasuda, H. Nishimura, T. Norimatsu, A. Sunahara, K. Nishihara, N. Miyanaga, Y. Izawa, K. Mima, Appl. Phys. Lett. **92**, 111 503 (2008)